Research Article | Vol. 7, No. 11 | 1 Nov 2017 | OPTICAL MATERIALS EXPRESS 3963
Optical Materials EXPRESS

Gain optimization, bleaching, and e-beam structuring of IR-140 doped PMMA and integration with plasmonic waveguides

MAUDE AMYOT-BOURGEOIS,[1,2] ELHAM KARAMI KESHMARZI,[2,3] CHOLOONG HAHN,[2,4] R. NIALL TAIT,[3] AND PIERRE BERINI[1,2,4,*]

[1]*Department of Physics, University of Ottawa, Ottawa, K1N 6N5, Canada*
[2]*Centre for Research in Photonics at the University of Ottawa, Ottawa, K1N 6N5, Canada*
[3]*Department of Electronics, Carleton University, 1125 Colonel by Dr., Ottawa, K1S 5B6, Canada*
[4]*School of Electrical Engineering and Computer Science, University of Ottawa, 800 King Edward Ave., Ottawa, K1N 6N5, Canada*
**berini@eecs.uottawa.ca*

Abstract: The optimal IR-140 weight ratio concentration producing maximum gain in amplified spontaneous emission measurements in the near-infrared (~880 nm) is determined. The structures investigated consist of PMMA polymer thin films, doped with IR-140 dye molecules in 4 different concentrations (0.7%, 0.8%, 0.9% and 1.0%), spin-coated on a silica layer grown on silicon wafers. The maximum material gain was obtained for the 0.9% weight ratio sample. The polarization dependence of the gain medium was also investigated, and the gain found to be similar in the TE and TM orientations. Bleaching of the gain medium, characterized by a decrease in the material gain due to pumping, was also explored and found to be rapid for thin films. However, bleaching is reduced as the pump energy density is reduced, creating a trade-off between gain and film longevity. The bleaching disappears at a low pump repetition rate. The gain films were structured via e-beam lithography to demonstrate the feasibility of this method for integration of structured doped polymers within optical devices. Amplification of the long-range surface plasmon guided by a gold stripe covered by the gain medium is also demonstrated and the modal gain measured was measured (~65 cm^{-1}) from which the material gain was deduced (~300 cm^{-1}). The material should prove useful for demonstrating device ideas and concepts in plasmonics and nano-photonics.

OCIS codes: (130.0130) Integrated optics; (160.0160) Materials; (220.0220) Optical design and fabrication; (310.0310) Thin films.

References and links

1. F. J. Duarte and L. W. Hillman, *Dye Laser Principles with Applications* (Academic Press, 1990).
2. S. Singh, V. R. Kanetkar, G. Sridhar, V. Muthuswamy, and K. Raja, "Solid-state polymeric dye lasers," J. Lumin. **101**, 285–291 (2003).
3. M. D. McGehee, R. Gupta, S. Veenstra, E. K. Miller, M. A. Diaz-Garcia, and A. J. Heeger, "Amplified spontaneous emission from photopumped films of a conjugated polymer," Phys. Rev. B **58**(11), 7035 (1998).
4. K. Yamashita, T. Kuro, K. Oe, and H. Yanagi, "Low threshold amplified spontaneous emission from near-infrared dye-doped polymeric waveguide," Appl. Phys. Lett. **88**(24), 241110 (2006).
5. J. Gosciniak and S. I. Bozhevólnyi, "Performance of thermo-optic components based on dielectric-loaded surface plasmon polaritons waveguides," Sci. Rep. **3**, 1803 (2013).
6. B. F. Howell and M. G. Kuzyk, "Amplified spontaneous emission and recoverable photodegradation in polymer doped with Disperse Orange 11," J. Opt. Soc. Am. B **19**(8), 1790–1793 (2002).
7. A. Costela, O. García, L. Cerdán, I. García-Moreno, and R. Sastre, "Amplified spontaneous emission and optical gain measurements from pyrromethene 567-doped polymer waveguides and quasi-waveguides," Opt. Express **16**(10), 7023–7036 (2008).
8. G. Somasundaram and A. Ramalingam, "Gain studies of Rhodamine 6G dye doped polymer laser," J. Photochem. Photobiol. Chem. **125**(1), 93–98 (1999).
9. T. Y. Tou, S. S. Yap, O. H. Chin, and S. W. Ng, "Optimization of a Rhodamine 6G-doped PMMA thin-slab laser," Opt. Mater. **29**(8), 963–969 (2007).

#300738 https://doi.org/10.1364/OME.7.003963
Journal © 2017 Received 23 Jun 2017; revised 29 Sep 2017; accepted 6 Oct 2017; published 19 Oct 2017

Optical Materials EXPRESS

10. J. Thompson, M. Anni, S. Lattante, D. Pisignano, R. I. Blyth, G. Gigli, and R. Cingolani, "Amplified spontaneous emission in the near infrared from a dye-doped polymer thin film," Synth. Met. **143**, 305 (2004).
11. E. K. Keshmarzi, R. N. Tait, and P. Berini, "Near infrared amplified spontaneous emission in a dye-doped polymeric waveguide for active plasmonic applications," Opt. Express **22**(10), 12452–12460 (2014).
12. A. N. Sudarkin and P. A. Demkovich, "Excitation of surface electromagnetic waves on the boundary of a metal with an amplifying medium," Sov. Phys. Tech. Phys. **34**(7), 764–766 (1988).
13. J. Seidel, S. Grafström, and L. Eng, "Stimulated Emission of Surface Plasmons at the Interface between a Silver Film and an Optically Pumped Dye Solution," Phys. Rev. Lett. **94**(17), 177401 (2005).
14. M. A. Noginov, "Compensation of surface plasmon loss by gain in dielectric medium," J. Nanophotonics **2**(1), 021855 (2008).
15. M. A. Noginov, G. Zhu, M. Mayy, B. A. Ritzo, N. Noginova, and V. A. Podolskiy, "Stimulated Emission of Surface Plasmon Polaritons," Phys. Rev. Lett. **101**(22), 226806 (2008).
16. P. M. Bolger, W. Dickson, A. V. Krasavin, L. Liebscher, S. G. Hickey, D. V. Skryabin, and A. V. Zayats, "Amplified spontaneous emission of surface plasmon polaritons and limitations on the increase of their propagation length," Opt. Lett. **35**(8), 1197–1199 (2010).
17. M. C. Gather, K. Meerholz, N. Danz, and K. Leosson, "Net optical gain in a plasmonic waveguide embedded in a fluorescent polymer," Nat. Photonics **4**, 457–461 (2010).
18. I. De Leon and P. Berini, "Amplification of long-range surface plasmons by a dipolar gain medium," Nat. Photonics **4**, 382 (2010).
19. C. Hahn, S. H. Song, C. H. Oh, and P. Berini, "Plasmonic gain in long-range surface plasmon polariton waveguides bounded symmetrically by dye-doped polymer," Appl. Phys. Lett. **107**(12), 121107 (2015).
20. S. Jetté-Charbonneau and P. Berini, "External cavity laser using a long-range surface plasmon grating as a distributed Bragg reflector," Appl. Phys. Lett. **91**(18), 181114 (2007).
21. E. Karami Keshmarzi, R. N. Tait, and P. Berini, "Long-range surface plasmon single-mode laser concepts," J. Appl. Phys. **112**(6), 063115 (2012).
22. D. J. Bergman and M. I. Stockman, "Surface Plasmon Amplification by Stimulated Emission of Radiation: Quantum Generation of Coherent Surface Plasmons in Nanosystems," Phys. Rev. Lett. **90**(2), 027402 (2003).
23. A. Boltasseva, T. Nikolajsen, K. Leosson, K. Kjaer, M. S. Larsen, and S. I. Bozhevólnyi, "Integrated optical components utilizing Long-Range Surface Plasmon Polaritons," J. Lightwave Technol. **23**(1), 413–422 (2005).
24. S. L. Clark, E. S. Handy, M. F. Rubner, and P. T. Hammond, "Creating Microstructures of Luminescent Organic Thin Films Using Layer-by-Layer Assembly," Adv. Mater. **11**(12), 1031–1035 (1999).
25. C. D. Müller, A. Falcou, N. Reckefuss, M. Rojahn, V. Wiederhirn, P. Rudati, H. Frohne, O. Nuyken, H. Becker, and K. Meerholz, "Multi-colour organic light-emitting displays by solution processing," Nature **421**(6925), 829–833 (2003).
26. Y. Oki, T. Yoshiura, Y. Chisaki, and M. Maeda, "Fabrication of a distributed-feedback dye laser with a grating structure in its plastic waveguide," Appl. Opt. **41**(24), 5030–5035 (2002).
27. M. B. Christiansen, M. Schøler, S. Balslev, R. B. Nielsen, D. H. Petersen, and A. Kristensen, "Wafer-scale fabrication of polymer distributed feedback lasers," J. Vac. Sci. Technol. B **24**(6), 3252–3257 (2006).
28. S. K. Vanga and A. A. Bettiol, "Proton beam writing of dye doped polymer microlasers," Nucl. Instrum. Methods Phys. Res. B **348**, 209–212 (2015).
29. Y. Che, O. Sugihara, H. Nakayama, and N. Okamoto, "Study on Electron Beam Lithography with Dye- Doped Polymer Material," Mol. Cryst. Liq. Cryst. Sci. Technol. Sect. A. **316**(1), 381–384 (1998).
30. S. Balslev, T. Rsmussen, P. Shi, and A. Kristensen, "Single mode solid state distributed feedback dye laser fabricated by gray scale electron beam lithography on a dye doped SU-8 resist," J. Micromech. Microeng. **15**, 2456–2460 (2005).
31. I. H. Malitson, "Interspecimen comparison of the refractive index of fused silica," J. Opt. Soc. Am. **55**, 1205–1208 (1965).
32. L. Dal Negro, P. Bettotti, M. Cazzanelli, D. Pacifici, and L. Pavesi, "Applicability conditions and experimental analysis of the variable stripe length method for gain measurements," Opt. Commun. **229**, 337–348 (2004).
33. I. De Leon and P. Berini, "Measuring gain and noise in active long-range surface plasmon-polariton waveguides," Rev. Sci. Instrum. **82**(3), 033107 (2011).
34. D. G. Cahill and R. O. Pohl, "Thermal conductivity of amorphous solids above the plateau," Phys. Rev. B Condens. Matter **35**(8), 4067–4073 (1987).
35. S. Popov, "Influence of pump repetition rate on dye photostability in a solid-state dye laser with a polymeric gain medium," Pure Appl. Opt. **7**(6), 1379–1388 (1998).
36. Z. Zhao, O. Mhibik, T. Leang, S. Forget, and S. Chénais, "Thermal effects in thin-film organic solid-state lasers," Opt. Express **22**(24), 30092–30107 (2014).
37. D. Nilsson, S. Balslev, M. M. Gregersen, and A. Kristensen, "Microfabricated solid-state dye lasers based on a photodefinable polymer," Appl. Opt. **44**(23), 4965–4971 (2005).
38. I. De Leon and P. Berini, "Spontaneous emission in long-range surrface plasmon-polariton amplifiers," Phys. Rev. B **83**(8), 81414 (2011).
39. R. Buckley and P. Berini, "Figures of merit for 2D surface plasmon waveguides and application to metal stripes," Opt. Express **15**(19), 12174–12182 (2007).
40. A. D. Rakic, A. B. Djurisic, J. M. Elazar, and M. L. Majewski, "Optical properties of metallic films for vertical-cavity optoelectronic devices," Appl. Opt. **37**(22), 5271–5283 (1998).

Optical Materials EXPRESS

1. Introduction

Solid state gain media are favorable compared to gain media in solution, as they do not present any issues brought by flowing liquids such as the need for fluidic channels, irregular flow rate or evaporation. Polymers doped with a laser dye are interesting because of the ease with which they are integrated with other materials and optical structures as an optically-pumped solid-state high-gain material [1,2]. Much research has been conducted on amplified spontaneous emission (ASE) gain from doped polymers in the visible range such as conjugated polymer BuEH-PPV [3], or in the near-infrared (NIR) such as poly(vinyl-pyrrolidone) (PVP) doped with LDS798 [4].

A polymer of particularly strong interest is poly(methyl metacrylate) (PMMA) for its low cost and ease of fabrication through well-known spin-coating and curing processes. Furthermore, its chained molecular structure makes PMMA a common choice amongst positive tone resists used for electron-beam lithography in nanofabrication of waveguides, gratings and other nanostructures. Other qualities worth mentioning are its good optical transparency and high thermo-optic coefficient ($\partial n/\partial T = -1.1 \times 10^{-4}$ K^{-1}) [5], making it a good candidate as a solid-state polymer for thermally-tunable optical components. ASE gain studies in the visible range have been performed on PMMA doped with various dyes such as Disperse Orange 11 [6], pyrromethene 567 [7], and Rhodamine 6G (R6G) [8,9], but there are few studies of ASE in dye-doped PMMA in the NIR. The organic dye IR-140 is an attractive option as an active dopant in the NIR because its wide emission spectrum peaks around 880 nm. A previous study integrated IR-140 in a PMMA polymer matrix to study ASE, reporting a material gain of 6.6 cm^{-1} at an emission wavelength varying from 920 to 970 nm [10]. Recently we investigated the effects of dye concentration and pump energy density on the gain obtained from IR-140 dye-doped PMMA films used as slab waveguides [11], and found a good molecular weight (m.w.) ratio of 0.8%, producing a maximum ASE gain of 68 cm^{-1}.

Long-range surface plasmon polaritons (LRSPPs) are surface waves propagating along a thin metal film in dielectric. One limitation to the application of LRSPPs (SPPs in general) is the propagation loss. It has been proposed to compensate the loss of SPP modes by using a gain medium as a cladding [12]. Since then, numerous studies have been performed on loss compensation, amplification and stimulated emission of SPPs [13–17]. The SPP propagation losses generally drop as the wavelength increases due to a reduction of the metal absorption and a decrease in confinement. Therefore, the overcompensation of SPP loss (*i.e.*, SPP amplification) is easier to achieve in the NIR. One study selected IR-140 as the dopant, in a solution consisting of a mixture of ethylene glycol and dimethyl sulphoxide, to cover a 1 μm wide gold waveguide, and the structure was pumped optically from the top to produce LRSPP amplification [18]. A subsequent study investigated LRSPP gain on a thin silver film symmetrically bounded by two layers of IR-140 dye-doped PMMA [19]. LRSPPs have a lower attenuation than SPP waves, and because of this, LRSPPs are good candidates towards the realization of high-quality single-mode plasmonic lasers [20,21] (spasers [22]) or other active devices based on integrated elements [23].

The nanostructuring of doped polymer films is an interesting approach to the fabrication of active devices such as Bragg-based lasers and micro-ring lasers. There exists a few techniques for patterning doped (and passive) polymers, each with its challenges, drawbacks, and advantages. A non-lithographic process following a bottom-up patterning approach has been used for ruthenium dye doped polymer, selectively deposited using indirect microcontact printing and multiple layer assembly, although the surface selectivity obtained for layering was low [24]. In another study, blue, red and green emitting dyes in polymer were patterned using mask photolithography [25]. The negative photolithography process produced photo-crosslinking in the polymer structures, rendering it insoluble. Post-exposure characterizations showed no alteration in the optical emission from the patterned polymer, but limitations of photolithography include polymer degradation, such as photo-oxidation, and

Optical Materials EXPRESS

(generally) low resolution of defined structures. Another method for polymer patterning consists of using two interfering UV beams to form a periodic structure, for example a grating, followed by wet etching. In a study using this interference lithography technique [26], distributed feedback (DFB) lasers were fabricated using two processes: Type 1 had its grating directly patterned on R6G doped PMMA, while type 2 had its grating defined on the passive substrate, which was then coated with the doped PMMA. The output laser emission from these 2 DFB devices were similar, although it was observed that type 1 had a shorter lifetime, attributed to dye degradation during UV exposure. Another nanostructuring technique for polymers, nanoimprint lithography (NIL), consists in the direct pressing of a stamp against a polymer. The imprinted shape can be maintained through thermal processing or UV curing. DFB lasers based on a Bragg grating modulated by periodic surface corrugations were fabricated using R6G doped PMMA, patterned following the thermal NIL technique [27]. The resulting DFB devices emitted laser radiation in a single mode at a wavelength dependent on the grating period. Proton beam writing (PBW) is a direct writing method that allows patterning of positive and negative resists. The polymer SU-8 is a negative resist that crosslinks under proton irradiation. Post exposure, the unexposed areas are chemically removed. Rhodamine B (RhB) doped SU-8 was used for the fabrication of microlasers using PBW [28]. A redshift was observed in the irradiated RhB doped SU-8 emission spectrum, compared to the un-irradiated sample, attributed to the effects of the proton beam on the material structure.

Electron beam lithography (EBL) is a direct writing nano-patterning method that has a much higher resolution than photolithography and that does not require hard masks, enabling fast turnaround of samples for research and prototyping purposes. A diffraction grating in Disperse Red 1 dye doped PMMA was fabricated using EBL, and the change in the absorption spectrum of the gain medium was investigated [29]. It was found that for higher exposure dosage, the absorption spectrum decreased and blue-shifted. This was linked to the intense electron bombardment of the material, breaking N-N bonds present in Disperse Red 1 molecules. In another study, DFB lasers were fabricated from R6G doped SU-8, which is a negative resist polymer, using the EBL gray-scale lithography [30]. The lasers were designed as Bragg waveguides with a periodic modulation coming from the nanometer scale thickness variation between two adjacent sections. The fabricated structures produced low threshold single mode lasing with an emission wavelength that was depending on the modulation pitch.

This paper builds on our previous work [11], investigating the potential and properties of IR-140 dye as an active dopant in PMMA (Poly(methyl methacrylate)) for LRSPP amplifiers and lasers. We give passive n and k measurements for some concentration ratios of IR-140 obtained using ellipsometry. We investigate the gain performance of thin films (1 μm), close to the thickness of the gain medium required in recently-proposed LRSPP lasers [22], by carrying out amplified spontaneous emission (ASE) measurements. Four concentrations of IR-140 in PMMA were tested and compared for different pump intensities, leading to optimal parameters maximizing the material gain available from this system. The polarization dependence of the gain is also investigated. Furthermore, using a set-up comprising a spectrograph and a high-speed intensified camera we acquire a sequence of individual single-pulse measurements allowing an accurate assessment of the photo-bleaching of the films. Different factors influencing the bleaching, such as the film thickness, the pump intensity and the pump repetition rate, are investigated. We also study the effects of prolonged thermal bakes on doped PMMA. We then study the effects of EBL on IR-140 dye-doped PMMA to investigate the viability of active nanostructures fabricated using this method. We design and fabricate straight waveguides with the EBL method, using constant exposure parameters except the dosage (total charge received per unit area) and we measure the material gain as a function of the exposure dosage. We further fabricate and test straight gold waveguides asymmetrically bound by SiO_2 and IR-140 doped PMMA and measure the modal gain of the LRSPP thereon.

Optical Materials EXPRESS

2. Structures and approaches

The structure of interest, sketched in Fig. 1(b), consists of a film of PMMA doped with IR-140, supported by a layer of SiO_2 and covered by air. The film is inserted in a variable slit length (VSL) set-up, as sketched in Fig. 1(a), which varies the length of the pumped waveguide section while monitoring the output intensity to extract the modal gain via ASE (discussed in detail below). The experiments were conducted on PMMA films of two different thicknesses: t_{PMMA} = 4 and 1 µm, of different IR-140 concentrations (0.7%, 0.8%, 0.9% and 1.0%) and for varying pump intensities. An investigation of the ASE polarization is carried out, as well as a study of the bleaching for both film thicknesses. Figure 1(c) shows the output facet of a sample, captured using an IR-camera under pumping, revealing the ASE signal generated in the structure (and showing some directly scattered pump light).

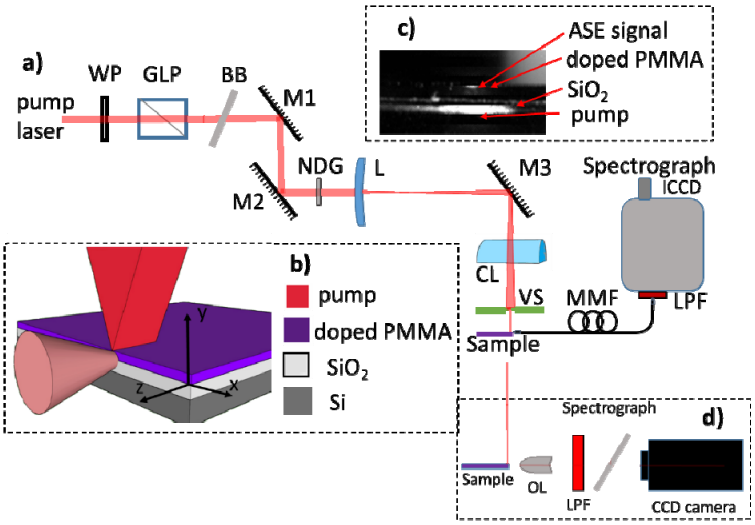

Fig. 1. (a) Experimental setup. WP: wave plate; GLP: Glan-Laser Polarizer; BB: motorized beam blank; M_i: silver mirrors; NDG: neutral density glass; L: plano-convex lens; CL: cylindrical lens; VS: variable slit; MMF: multimode fiber; LPF: 850 nm long pass filter. (b) Sketch of a sample structure with pump stripe and ASE signal. A coordinate system was added for clarity. The pump stripe length extends along the z axis. (c) Imaging of the ASE signal with a CCD camera. (d) Alternative setup allowing spectrum and image acquisition simultaneously.

The variable slit length method used to measure the gain in the doped medium gives the modal gain g_{mod}, from the intensity equation:

$$\frac{dI_{ASE}}{dz} = \left(CF \times g_{mat} - \alpha\right) I + J = g_{mod} I + J \tag{1}$$

where I_{ASE} is the ASE signal intensity, J is the photon spontaneous emission factor, g_{mat} and g_{mod} are respectively the material and modal gains, and α, the attenuation constant, is neglected due to the low propagation loss encountered over short distances z. g_{mat} can then be extracted from:

$$g_{mat} = g_{mod} / CF \tag{2}$$

The confinement factor (CF) of this structure is defined as the ratio of the mode power in the doped PMMA layer to the total mode power in the structure (PMMA, air and SiO_2) and can be expressed as:

Optical Materials EXPRESS

$$CF = \int_0^{t_{PMMA}} S_{ave}\,dy \Big/ \int_{-\infty}^{\infty} S_{ave}\,dy \tag{3}$$

where t_{PMMA} is the doped PMMA layer thickness (along the y axis) and S_{ave} is the power density associated with the TE_0 mode (E_x) or TM_0 mode (E_y), expressed as:

$$S_{ave} = \frac{1}{2} Re\left\{(\bar{E} \times \bar{H}) \cdot \hat{z}\right\} \tag{4}$$

The CF was calculated numerically from the electric field norm distributed over the device cross-section, obtained from finite-element modelling of the vector wave equations (Comsol), then discretizing the integration domain into finite elements on which the electric field magnitude E_x or E_y were extracted.

Figure 2(a) shows the distribution of the E_x and E_y fields as they vary along the y coordinate for a sample wafer with a PMMA layer thickness of 1 µm. At this thickness the confinement of the slab modes propagating therein is not very high and a non-negligible portion of the fields propagate in the passive substrate (of lower refractive index than the active film). The calculated CF of each specific structure is given in Tables 1 and 2. These calculated values of CF are used to calculate g_{mat} from the measured g_{mod} in each structure characterized as described above.

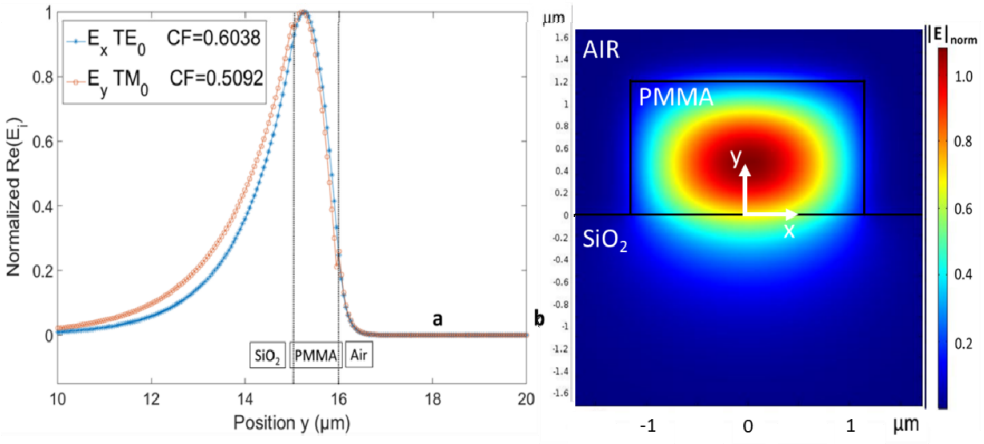

Fig. 2. (a) Distribution of the normalized electric field magnitude along the y axis of the film structure (slab waveguide). CF is the confinement factor calculated for the TM_0 and TE_0 modes for the case t_{PMMA} = 1 µm. (b) Fundamental guided TM mode in a doped PMMA ridge waveguide of thickness t = 1.3 µm and width w = 2.3 µm on SiO_2; distribution of the $|E_y|$ field.

Single-mode ridge waveguides in IR-140 doped PMMA are needed for the portion of our study pertaining to the effects of EBL on the gain of the medium. For this purpose, ridge dimensions were determined numerically using Comsol. For IR-140 concentrations of 0.8% and 0.9% in PMMA, the refractive indices at λ = 880 nm are respectively n = 1.505 + i0.000504 and n = 1.509 + i0.000567 (where the real part was extracted from the ellipsometry measurements, given in Fig. 3(a) and the imaginary part represents the gain and is extracted from the material gain results described in Section 4.2 using $\kappa = \lambda g_{mat}/(2*2\pi)$). The PMMA layer is formed on thermally grown SiO_2 (n = 1.4521 [31]) covered by air, as sketched in Fig. 2(b), and the dimensions to support a single TM mode were found to be w = 2.3 µm for the width and a thickness of t = 1.3 µm. The confinement factor for this arrangement, calculated using the method described previously but extended to two dimensions, is CF = 0.8757 for the fundamental TM mode.

Optical Materials EXPRESS

Ellipsometry measurements were obtained on dye-doped PMMA films of a thickness of 360 nm for an IR-140 dye concentration varying from 0.0% to 1.0% (% weight) in order to characterize the dispersion of the films. The ellipsometer used was the UVISEL spectroscopic ellipsometer from HORIBA and the acquired data were then fit to a double-amorphous model. Figure 3 gives the results obtained from these measurements.

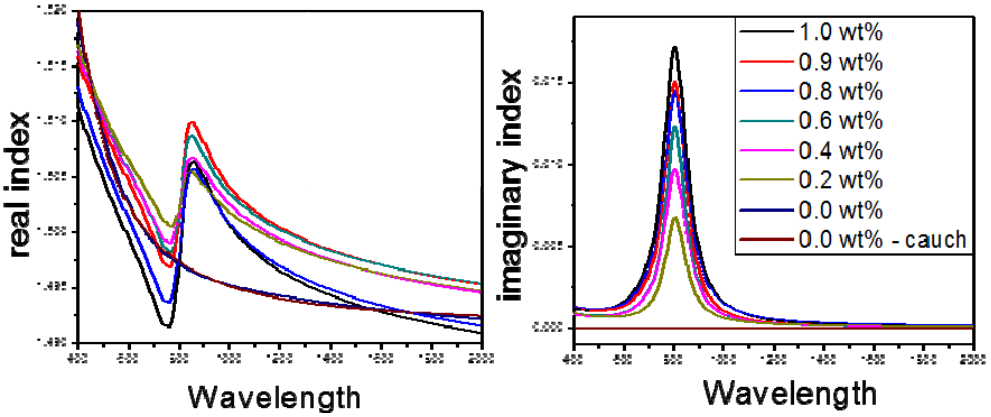

Fig. 3. Dispersion of IR-140 doped PMMA as a function of dye concentration (wt%).

The data points for 0.8% and 0.9% at λ = 880 nm correspond to a real refractive index of n = 1.505 and n = 1.509, respectively for doped PMMA, and these values were used in the numerical analysis of the slab modes and ridge waveguides (above). We note from Fig. 3(b) the absorption of IR-140 which peaks near 820 nm. The magnitude of the absorption increases with IR-140 concentration as expected. Significant dispersion is also evident in the real part of the refractive index (n) near 800 nm due to IR-140, as shown in Fig. 3(a).

3. Slab waveguide fabrication

Previously, dye-doped PMMA films with dye molecular weight (m.w.) ratios of 0.4%, 0.8%, 1.2% and 1.6% were fabricated and tested, and it was found that the 0.8% concentration film produced the highest material gain among this set [11]. Therefore, here we limit our concentrations to near 0.8% in order to determine an optimum. Four weight ratios of IR-140 to PMMA solids were selected as 0.7% (4.6×10^{18} cm^{-3} molecular conc.), 0.8% (5.2×10^{18} cm^{-3}), 0.9% (5.9×10^{18} cm^{-3}) and 1% (6.5×10^{18} cm^{-3}). The IR-140 dye has a broad absorption peak around 820 nm (Fig. 3(b)) and a narrower fluorescence emission peak around 880 nm (shown below). The IR-140 dye was diluted in PMMA dissolved in dichloroethane. The four different dye-doped PMMA solutions were then spin-coated on a 15 µm thick SiO_2 layer on 500 µm thick Si substrates. The spinning speed (RPM) determines the final thickness of the doped PMMA layer on the wafers. They were then cured for 3 minutes at 180 °C on a hotplate. To avoid the effects resulting from the edge bead created during the spinning process, the wafers were carefully cleaved and then cleaned with isopropyl alcohol. The ASE emission was collected from the clean cleaved edges near the center of the wafers.

The thickness of each film was measured using a Dektak profilometer. The sample under test was first scratched along two edges to remove the PMMA layer and create a reference level along the top surface of the SiO_2. Then, a scan was performed monitoring the PMMA thickness from one scratch to the other, assuming the SiO_2 height is uniform. The thickness of films 0.7%, 0.8%, 0.9%, 1.0%, and a thin version with 0.8%, were, respectively, 4, 3.9, 4, 3.7 and 0.96 µm, and the average standard deviation of the thicknesses of this set was 40 nm.

Optical Materials EXPRESS

4. Experimental methods and results for slab waveguides

4.1 Spontaneous emission (SE)

The four samples of different IR-140 concentration were pumped using a Centennia CW laser system emitting at 532 nm. A small fraction of the beam power was coupled into a multimode fiber and redirected to a 10 × objective to focus the beam onto the top surface of a sample. The spontaneous emission was collected from a cleaved edge using a multimode fiber and sent to an optical spectrum analyzer, (Newport, OSM2-400VIS/NIR). A SE spectrum is shown in the inset of Fig. 4, revealing a peak emission near 880 nm and a FWHM of 60 nm.

4.2 Gain measurements

The pump signal for the gain measurements was generated via a Cobra Stretch Sirah pulsed dye laser system using a solution of styryl dye emitting at 810 nm, with a repetition rate of 10 Hz. A detailed schematic of the experimental setup is shown in Fig. 1(a). The pump beam after attenuation (NDG) was expanded with a lens (L), then a mirror (M3) directed the beam down towards the sample through a cylindrical lens (CL) to transform the circular pump beam into a narrow pump stripe oriented along the z direction of the sample (Fig. 1(b)).

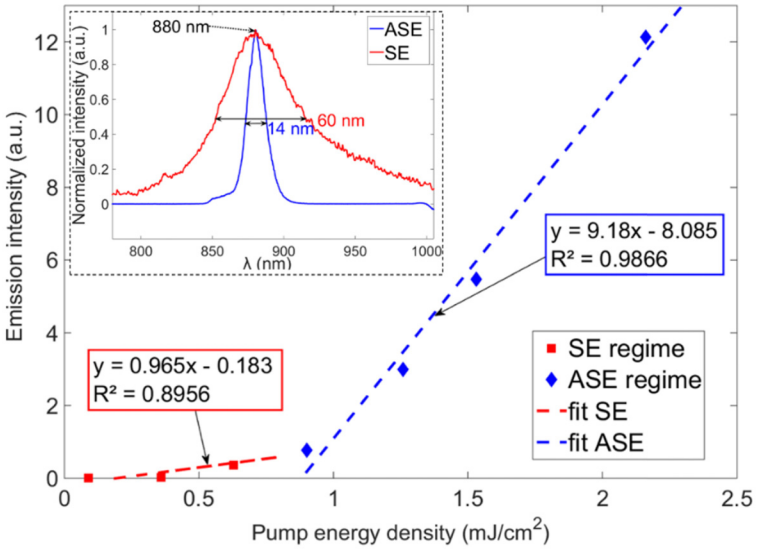

Fig. 4. Emission intensity as a function of pump energy density, showing the energy threshold for ASE. Inset: comparison between fluorescence (SE, low pump energy density) and ASE (pump energy density E_p = 3.6 mJcm^{-2}) spectra. Sample: 0.9% IR-140 and t_{PMMA} = 4 µm.

The sample distance from the cylindrical lens was chosen such that the pump stripe width measures 100 to 150 µm. The pump polarization was aligned parallel to the length of the pump stripe (z axis) throughout the experiments because it is in this orientation that the TM mode has the strongest gain coefficient and emission intensity (SPP waves are TM in nature) which is important for plasmonic applications, whereas the ASE emission is strongly TE polarized if the pump polarization is perpendicular to the length of the pump stripe [11].

The variable slit (VS) was placed near the sample to reduce diffraction effects from the pump beam [32]. The VS was constructed from a micrometer-controlled movable blade and a fixed blade. The slit width can be varied from 0 to 3 mm. The relation between the VS width and the actual stripe length was determined using photosensitive photographic paper by measuring the stripe length from the burn edges on the paper for various slit widths. A linear model relating the stripe length to the slit width was used for the gain measurements.

Optical Materials EXPRESS

Homogeneity of the pump stripe is a key factor for good gain measurements [32,33]. The homogeneity of the pump stripe intensity over its length was tested by measuring the pump stripe power incident on the sample position using a power meter for various openings of the slit, thus varying the stripe length. A homogeneous stripe has a constant intensity along its length, thus a constant ratio of power-to-length over the stripe length (all other variables being constant). It was found that the power would vary by a factor of 3% on average, showing a homogeneous pump source.

The sample was placed such that the cleaved edge was at the end of the pump stripe and the two overlapped. A pump stripe that ends before the edge of the sample would reduce ASE signal collection considerably due to absorption in the unpumped gain region.

The signal emitted from the sample was sent to the spectrograph (Princeton Instruments IsoPlane SCT320, PI-MAX4 ICCD camera). The ICCD camera was linked to the YAG laser trigger to synchronize the camera shutter to the pump laser pulses (the laser pulse width varies between 6 and 11 ns). This reduces noise and allows for pulse-to-pulse analysis.

ASE signals can be distinguished from SE signals by their spectra, as shown by the narrowing of the spectrum from 60 nm in the SE regime to 14 nm in the ASE regime, in the inset of Fig. 4. Another sign of evolution from SE to ASE is the rapid increase in signal emission intensity beyond a threshold pump energy density (stripe length remaining fixed), as shown in Fig. 4, revealing that the slope of I_{ASE} as a function of E_p is significantly larger (~10 ×) in the ASE regime compared to the SE regime.

The VSL method was used to determine the material gain for our four concentrations of IR-140 to PMMA. Integrating Eq. (1) over z from 0 to l and assuming $I_{ASE}(z = 0) = 0$ gives:

$$I_{ASE} = \frac{J}{g_{mod}}\left(e^{g_{mod}l} - 1\right) \tag{5}$$

Several sets of measurements of I_{ASE} as a function of pump stripe length l were fit to Eq. (5) for various E_p applied to each sample. The modal gain was extracted from these fitted equations. The results of these experiments along with the fitted curves are plotted in Figs. 5(a) and 5(c), for samples having 0.9% IR-140 and a thickness of t_{PMMA} = 4 μm, and 0.8% IR-140 and a thickness of t_{PMMA} = 1 μm, respectively. Each data point on the plots corresponds to the maximum intensity of an emission spectrum averaged over 40 acquisition pulses for a specific stripe length.

Table 1 gives the maximum modal gain obtained for each dye concentration at pump intensities below gain saturation. The optimal material gain was produced by the 0.9% m.w. IR-140 concentration at E_p = 4.1 mJ/cm^2, giving a material gain of g_{mat} = 81 cm^{-1}. This is a significant improvement over our previous maximum gain measured for a concentration of 0.8% (g_{mat} = 68 cm^{-1}) [11], confirmed here in Table 1 for the same concentration (g_{mat} = 70 cm^{-1} for the 4 μm thick film, and g_{mat} = 65 cm^{-1} for the 1 μm thick film). The CFs shown in Table 1 were calculated using the method previously described for TM and TE modes and averaged. The peak emission wavelength for each concentration is also displayed in Table 1, varying from 870 to 881 nm.

Table 1. Summary of measured modal and material gains for each sample at their optimal pump energy density; each sample is 4 μm thick except the last one which is 1 μm thick.

Conc., m.w.	E_p	g_{mod}	CF	g_{mat}	λ_{peak}
[%]	[mJcm^{-2}]	[cm^{-1}]		[cm^{-1}]	[nm]
0.7	4.1	72	1	72	876
0.8	4.5	70	1	70	876
0.9	4.1	81	1	81	881
1	4.1	62	1	62	881
0.8 t = 1 μm	4.78	36.2	0.557	65	870

Optical Materials EXPRESS

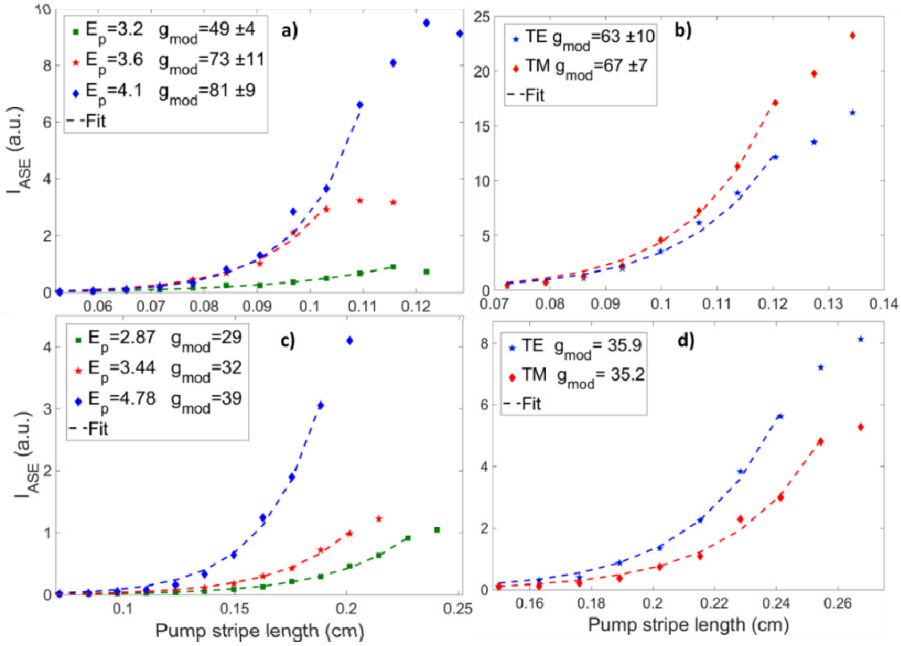

Fig. 5. (a) and (c): Emission intensities as a function of the stripe length for the sample with 0.9% IR-140 and a thickness of t_{PMMA} = 4 µm (a), and 0.8% IR-140 and a thickness of t_{PMMA} = 1 µm (c). (b) and (d): Emission intensities in the TM and TE orientations as a function of the stripe length for the sample with 0.9% IR-140 and a thickness of t_{PMMA} = 4 µm (b), and 0.8% IR-140 and a thickness of t_{PMMA} = 1 µm (d). The modal gain g_{mod} (in cm^{-1}) is obtained by fitting Eq. (6) to the measurements. Pump energy densities E_d are in mJ/cm^2.

4.3 Polarization study of ASE signal

SPP waves being TM polarized, it is important to determine the material gain that is available in the TM orientation. A polarization study was conducted to measure g_{mat} in the TM and TE polarizations. The pump polarization was kept parallel to the pump stripe since it is in this orientation that it was previously demonstrated to possess the strongest TM gain [11]. An analyzer was inserted before the MMF and oriented vertically (TM) or horizontally (TE) for the VSL experiments, measurements for each stripe length being obtained in the two orientations, sequentially. The fitted curves for these cases are shown in Figs. 5(b) and 5(d) for samples having 0.9% IR-140 and a thickness of t_{PMMA} = 4 µm, and 0.8% IR-140 and a thickness of t_{PMMA} = 1 µm, respectively. Table 2 gives the modal and material gains measured in the TE and TM orientations, along with CF calculated using the method previously described. For thick PMMA films the mode is well-confined to the PMMA layer but for thin films the confinement is reduced. The TE and TM material gains are observed to be similar.

Table 2. Summary of measured polarization-resolved modal and material gains for each sample at their optimal pump energy density; 0.9% sample is 4 µm thick while 0.8% sample is 1 µm thick.

Conc., m.w.	E_d	g_{mod}	CF	g_{mat}
	[$mJcm^{-2}$]	[cm^{-1}]		[cm^{-1}]
0.9% t = 4 µm TE	4.1	63	≈1	63
0.9% t = 4 µm TM	4.1	67	≈1	67
0.8% t = 1 µm TE	4.9	35.9	0.604	59.5
0.8% t = 1 µm TM	4.9	35.2	0.509	69.1

The discrepancy between the g_{mat} results given in Tables 1 and 2 for similar measurement conditions could be explained by the setup modifications to perform the polarization study.

Optical Materials EXPRESS

Indeed, an analyzer and an objective lens were added before the MMF and this addition could induce loss. Furthermore, the polarization study was performed a few weeks after the gain optimization study - the samples may have deteriorated slightly over time.

4.4 Bleaching tests

Dye molecules are known to degrade when exposed to intense light. While this property is of little consequence in liquid dye solutions with constant flow, it has major effects on a solid layer of PMMA doped with dye, reducing the gain obtained from the material after long exposure to the pump. Since applications depend on the life expectancy of dye molecules in a PMMA layer, the bleaching effect was investigated. The pump source used to perform the bleaching test was the same as for the gain measurements. Samples were exposed to different pump intensities below gain saturation, with a pump stripe length below signal saturation. The ASE signal was determined by averaging over 50 spectra to produce one data point (5 s at a pump laser repetition rate of 10 Hz). For a constant pump repetition rate at 10 Hz, it was found that the effects of bleaching are considerably reduced for thicker doped polymer films (4 μm) compared to thin films (1 μm) as seen in Fig. 6(a).

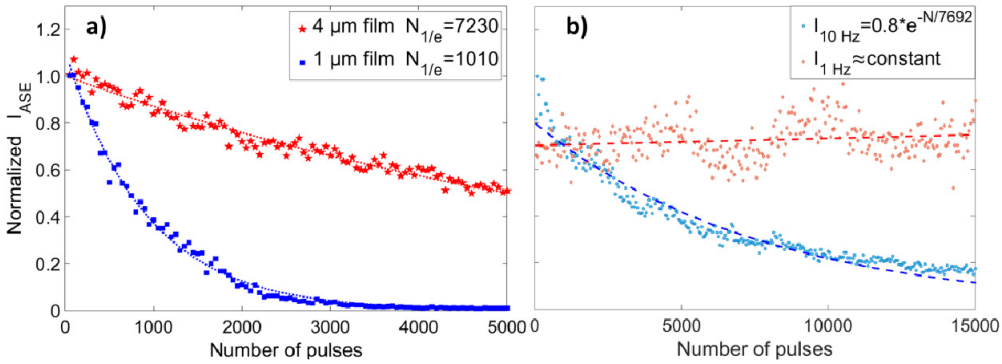

Fig. 6. (a) Bleaching curves of ASE signal for different PMMA film thicknesses (1 μm, 4 μm). The lifetime of emission $N_{1/e}$ given in the figure legend were calculated based on a fitted exponential decay. The pump energy density is kept at 6 mJ/cm^2. (b) Bleaching curves of ASE for a IR-140 dye doped PMMA film of thickness 680 nm for pump repetition rates of 10 and 1 Hz and a pump laser pulse energy of 0.4 mJ.

The curves for peak emission intensity as a function of the exposure time were extracted, and fitted to exponential curves:

$$I_{ASE}(t) = I_{ASE0} e^{-N/N_{1/e}} \tag{6}$$

The exposure pulse number corresponding to a 1/e reduction in signal intensity ($N_{1/e}$) was determined from these exponential curves. From the results shown in Fig. 6(a), it is seen that for a sample with a thick 4 μm layer of doped PMMA, bleaching is weak, with $N_{1/e}$ = 7230 (a lifetime of over 12 minutes at a repetition rate of 10 Hz). Samples with a thin 1 μm PMMA layer have a shorter life expectancy, with $N_{1/e}$ = 1010 (a lifetime of 100 s at a repetition rate of 10 Hz), but this lifetime can be increased if the pump energy density is decreased, indicating a trade-off between material gain and material lifetime.

The degradation of the samples is thought to be caused by thermal damage, due to the poor thermal conductivity of PMMA, of the order of 0.2 Wm^{-1}K^{-1} [34], resulting in a heat dissipation time of about 0.5 s [35]. Thus, the pump repetition rate has a great influence over the thermal degradation of polymer films. The lifetime of R6G dye-doped PMMA has been investigated at repetition rates of 4 and 10 Hz [35]. The lifetime of Rhodamine 640 doped PMMA was investigated at pump repetition rates of 50 to 200 Hz [36]. The lifetime of R6G

Optical Materials EXPRESS

doped SU-8 was investigated for pump repetition rates of 2.5 to 10 Hz [37]. In all cases it was shown that lower repetition rates exhibit lower bleaching and longer lifetimes.

We thus investigated the lifetime of IR-140 doped PMMA as a function of the pump repetition rate. The pump rates used were 10 Hz, which is the standard repetition rate of our pump laser, and 1 Hz, for which the time interval between pulses is longer than the PMMA heat dissipation time. For both sets of measurements, the pump laser pulse energy was kept to 0.4 mJ. The doped film of thickness 670 nm was exposed to over 15,000 pulses, and the peak intensity of the ASE spectra was averaged over 50 pulses (to reduce noise) and observe bleaching. The results given in Fig. 6(b) show that for the higher repetition rate (10 Hz), degradation of the sample was present and could be fitted to an exponential decay. The 1 Hz curve, on the contrary, appears constant, indicating the absence of bleaching at low repetition rates. The sinusoidal shape is attributed to drift in the experimental setup due to the long exposure (> 4 hrs).

4.5 Baking tests

Depending on the application, it is sometimes necessary to bake a structure comprising a doped polymer film for long periods of time. There is a possibility that the baking process inflict thermal damage to the doped polymer, reducing the available material gain. To test the effects of prolonged baking on IR-140 doped PMMA, doped films (0.9%) were made according to the fabrication process described previously, and spun to a thickness of t = 400 and 670 nm. The films were then cured for 3 minutes on a hotplate at a temperature of 180 °C. The films were then cleaved into three parts. One part was tested as is to obtain the modal and material gains, while the other parts were baked for 12 hours on a hotplate at 100 °C and 180 °C before testing. Table 3 lists the results from these experiments.

Table 3. Gain measured for different baking processes of IR-140 dye doped PMMA

film thickness	Cured only T = 180 °C 3min		T = 100 °C 12h		T = 180 °C 12h	
t [nm]	g_{mod} [cm^{-1}]	g_{mat} [cm^{-1}]	g_{mod} [cm^{-1}]	g_{mat} [cm^{-1}]	g_{mod} [cm^{-1}]	g_{mat} [cm^{-1}]
670	10.0	20.4	10.5	21.4	-	-

The confinement factor CF for each film was calculated using the previously described method, to extract the material gain. It was calculated to be CF = 0.495 for a thickness of 670 nm. One simple observation that is clear from Table 3 is that there is no significant gain difference between the samples that were cured for 3 minutes at T = 180 °C compared to those that were cured then baked for 12 hours at T = 100 °C, showing that such baking over a long period of time does not adversely affect the expected gain. All samples that were baked at T = 180 °C for 12 hrs produced no emission (SE or ASE), showing that a prolonged bake at high temperature (T = 180 °C) induces extensive thermal damage to the medium.

5. Experimental methods and results for ridge waveguides

5.1 Fabrication of ridge waveguides

The waveguide ridge dimensions were chosen as described above to achieve single TM mode guidance (w = 2.3 μm, t = 1.3 μm). IR-140 doped PMMA films (0.8%) were spun according to the process described above. The obtained film thickness was t = 1.33 μm, as measured by a profilometer. Straight waveguides were patterned using EBL. Since PMMA is a positive resist, the material surrounding the waveguides had to be exposed and removed by developing. The laser pump width is almost 200 μm, and it is undesirable for the slab region near the ridge to be pumped, so exposure regions 400 μm wide were designed near each ridge. The ridge waveguides are long, so the exposure areas are large. In order to reduce the exposure time, the surfaces were divided into three regions where various e-beam step sizes

Optical Materials EXPRESS

were applied: small for feature definition near the ridges, and increasingly large for clearing the doped PMMA around the structure. Figure 7(a) shows the exposure areas defined near each ridge shown in purple. The dosage, which is the total charge that a unit area receives, was the only exposure parameter varied: 96, 106, 115, 125 and 134 μC/cm^2 for ridges 1 to 5, respectively, for an e-beam aperture of 30 μm and an acceleration voltage of 10 kV. Figures 7(b) to 7(g) show fabricated ridge waveguides examined through optical microscope, AFM and SEM. Higher dosage ridge waveguides exhibit a waist cross-section, as shown in Figs. 7(f) and 7(g). These ridges still support guided modes with a confinement factor (0.8309) similar to that of an ideal rectangular ridge waveguide (0.8757), as found from numerical calculations. Lower dosage ridges exhibit a skirt-like cross-section as shown in Fig. 7(d) and (e), giving CF = 0.8710. Corresponding mode field distributions (E_y) for the fundamental TM mode were computed and are given to the right of each SEM cross-section.

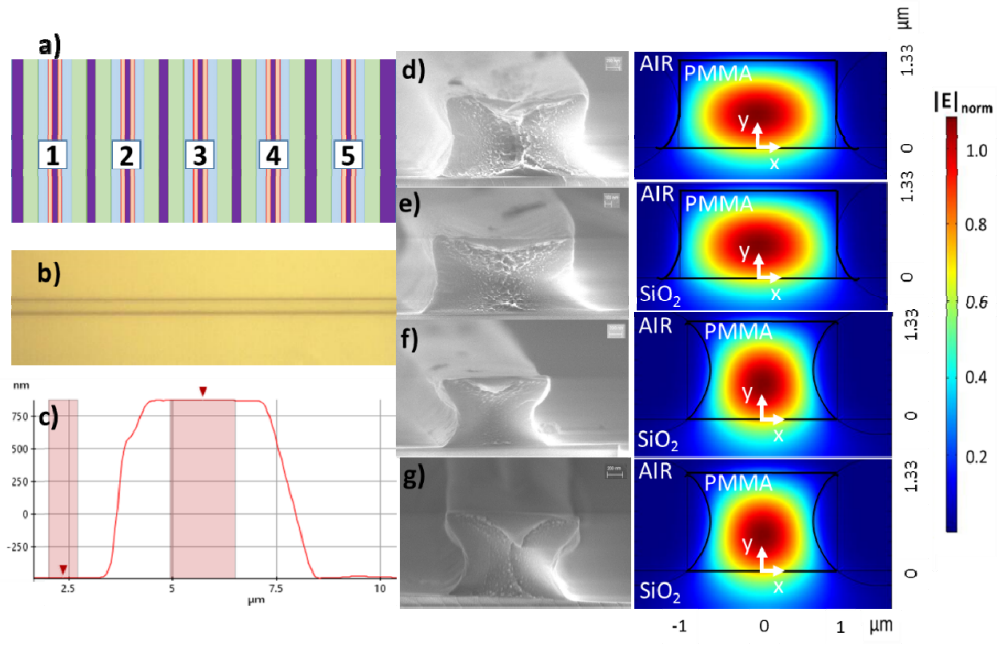

Fig. 7. (a) E-beam writing layout for ridge waveguides. Purple is doped PMMA whereas pink, blue and green are exposed areas with decreasing resolution. (b) Optical microscope image of one ridge waveguide. (c) AFM thickness profile of one waveguide; the surface roughness along the top of the ridge is ~9 nm (RMS). SEM cross-sectional images of waveguides and associated fundamental TM mode (computed) for doses of: (d) D = 96 μC/cm^2, (e) D = 106 μC/cm^2, (f) D = 115 μC/cm^2, (g) D = 134 μC/cm^2. The CF for cases (d) and (e) are CF = 0.8710, whereas for cases (f) and (g) are CF = 0.8309.

5.2 Experimental methods and results for ridge waveguides

A die was cleaved and the VSL method was performed to extract the modal gain for each ridge waveguide. The setup of Fig. 1(d) was used to observe simultaneously mode images on the infrared (IR) camera and emission spectra using the spectrometer. The pump was aligned to a narrow waveguide such that the image observed was brightest, with no slab guiding being observed, as shown in inset to Fig. 8(a). The modal gain was measured many times for the three ridge waveguides exposed to the lowest dosage, which was 96, 106 and 115 μC/cm^2, and the material gain was calculated using the confinement factor calculated numerically (as described above) of CF = 0.8710 for the two lowest dosage, and CF = 0.8309 for the highest. Example results are shown in Fig. 8(b).

Optical Materials EXPRESS

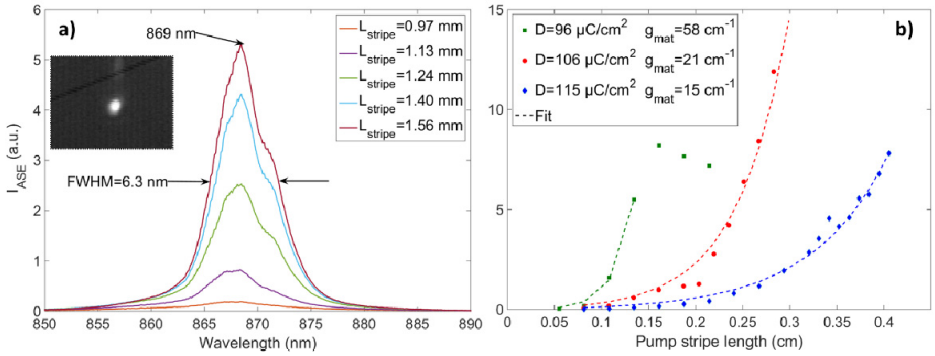

Fig. 8. (a) ASE spectra for several pump stripe lengths at a constant energy density. Inset: ridge waveguide mode image observed on a IR camera. (b) VSL results for three ridge waveguides created with different e-beam dosages.

The material gain measured for the film exposed with the lowest dose (58 cm^{-1}) is slightly reduced compared to that obtained for the corresponding slab waveguide (70 cm^{-1}). We also note that the material gain drops with increasing dose. The ridge waveguides patterned with the highest doses of 125 and 134 $\mu C/cm^2$, were all optically inactive (no signal was emitted from these waveguides). This indicates that the e-beam has an effect on the gain medium, and the electron flux should be minimized. Nonetheless, it is possible to structure IR-140 doped PMMA films using EBL, but high exposure doses reduce the material gain. These results should prove useful for designing and fabricating more complex active structures.

6. Experimental methods and results for plasmonic waveguides

6.1 Fabrication of plasmonic waveguides

Fabricated gold waveguides, following the cross-sectional sketch of Fig. 9(d), have a thickness t_{Au} = 19.4 nm (AFM) and a width w_{Au} = 1 μm (SEM). The substrate consisted of a t_{SiO2} = 15 μm thick layer of fused silica on Si, and the top cladding consisted of an IR-140 doped (0.9%) PMMA layer of thickness t_{PMMA} = 490 nm, below the cut-off thickness for guiding ASE slab modes (TE_0, TM_0).

The fabrication process is as follow: the waveguides were patterned using EBL on a PMMA resist bilayer that was later developed. The gold layer was evaporated and the resist layer was carefully lifted-off. The doped PMMA layer was then spun following the process described in Section 3, but with a curing temperature reduced to T = 170 °C. No adhesion layer was used between the gold stripes and the underlying SiO_2 cladding.

Optical Materials EXPRESS

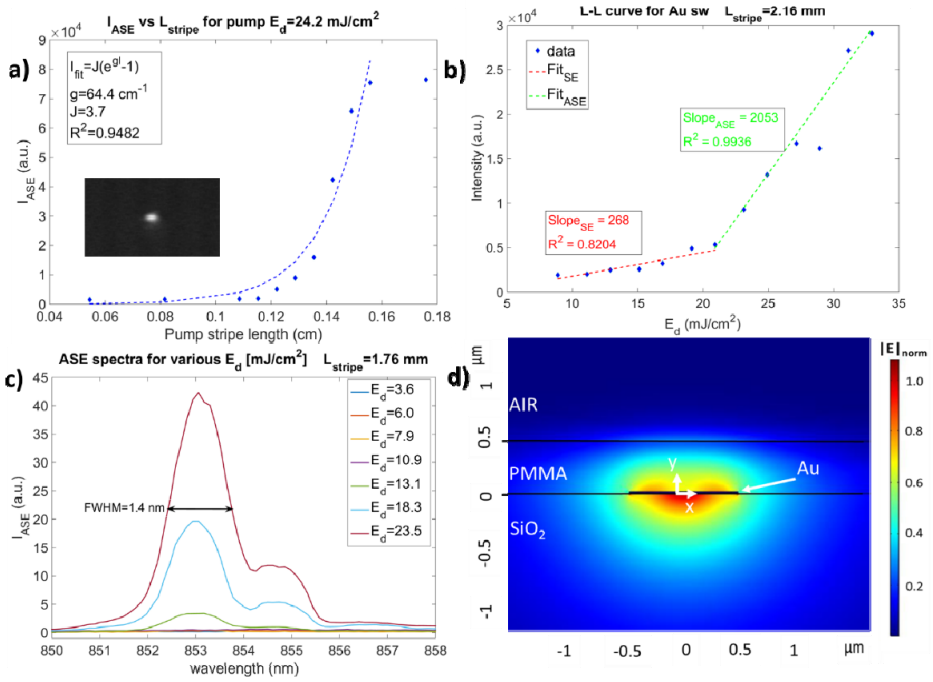

Fig. 9. (a) Cross-sectional sketch of a gold waveguide showing the normalised (computed) distribution of the E_y field component of the LRSPP mode. (b) ASE results obtained using the VSL method. Inset: ASE-LRSPP mode image. (c) LRSPP emission intensity as a function of the pump energy density for a fixed pump stripe length. (d) ASE-LRSPP spectra as a function of pump energy density (mJ/cm^2).

6.2 Experimental methods and results for plasmonic waveguides

The setup of Fig. 1(d) was used to observe simultaneously mode images on the infrared (IR) camera and emission spectra using the spectrometer. An analyzer in the TM orientation was placed in the set-up immediately beyond the waveguide output. The VSL method was applied to measure the modal gain of the LRSPP on the plasmonic waveguide. The results are shown in Fig. 9(a), from which a modal gain of g_{mod} = 64.4 cm^{-1} is deduced. This is 3 × larger than what was measured in a previous study for gold waveguides covered by IR-140 in solution [38]. A typical image of the mode output, acquired with the IR camera, is shown as the inset of Fig. 9(a). L-L measurements were also obtained to observe the threshold between SE and ASE, as shown in Fig. 9(b). It is observed that the threshold energy density is about 21 mJ/cm^2 at the location of the kink (which is clearly apparent). The slope of the ASE regime is about 10 × larger than that of the SE regime.

Figure 9(c) shows evolution of the output spectrum as the pump energy density is increased at a fixed pump length. It is worth noting that the peak wavelength (λ_{peak} = 853 nm) is appreciably blue-shifted relative to the slab modes (λ_{peak} = 870-881 nm, Table 1). The peak ASE emission is determined by the interplay between the gain spectrum, and the modal dispersion of the amplified mode, particularly its attenuation and confinement. For LRSPPs, modal confinement and attenuation increase together leading to a trade-off that can be quantified using figures of merit [39]. It is interesting to note that one of these figures of merit (M_2 - defined as the difference between the real modal effective index and the refractive index of the cladding divided by the imaginary part of the modal effective index), tends to peak near 850 nm for LRSPPs on gold stripes [39]. Using this definition, we compute that the LRSPP in our passive waveguide performs better at 850 nm than at 880 nm, which could explain the observed peak in ASE at 853 nm.

Optical Materials EXPRESS

For modelling purposes, the gold refractive index at the peak wavelength of λ_{peak} = 853 nm was taken as n = 0.22139 - i5.3141 [40], the fused silica refractive index was n = 1.4521 [31] and the 0.9% PMMA refractive index was n = 1.5059 + i0.002, where the real part is extracted from the ellipsometry measurements described in Section 2, while the imaginary part was fitted to the modal gain results shown in Fig. 9(a). Figure 9(d) shows the computed normalized electric field distribution of the LRSPP over the cross-section for which the computed effective refractive index was n_{eff} = 1.4585 + i4.322e-4. This result suggests a larger material gain (g_{mat} = 295 cm^{-1}) than what was measured in Section 4.2 (g_{mat} = 81 cm^{-1}) for the slabs, corresponding to a significant increase (~4 ×) in material gain relative to previous work [11]. The higher gain is explained through optimization of the dopant concentration and the processing parameters (including the use of fresh solutions and lower curing temperature).

7. Conclusion

The gain available in PMMA films doped with IR-140 dye molecules was investigated and a maximum material gain of g_{mat} = 295 cm^{-1} was measured for an optimal dye molecular weight concentration of 0.9%. The polarization of the ASE was studied and it was found that the ASE emission is unpolarized, so that the gain available in the TM orientation is sufficiently high to be useful for certain applications in plasmonics. The gain medium life expectancy was measured through a photo-bleaching study, and it was found that the bleaching was reduced for thicker films and disappeared completely for repetition rates lower than the PMMA heat dissipation time (< 2 Hz). The effect of prolonged baking on the gain was investigated, and no effect was observed for prolonged heating at 100 °C, but for prolonged heating at 180 °C the devices no longer emitted. This indicates that an active structure incorporating this medium should be processed at temperatures that are as low as possible. We investigated IR-140 doped PMMA ridge waveguides defined via EBL, and found that the material gain decreases with increasing e-beam exposure dose, until rendered inactive. Nevertheless, it is possible to define features in this medium using EBL without affecting too deleteriously the material gain. We integrated the doped PMMA medium into a plasmonic structure, namely gold stripe waveguides, and measured a LRSPP modal gain of g_{mod} = 64.4 cm^{-1}.

Acknowledgments

This work was performed at the new Centre for Research in Photonics of University of Ottawa (CRPuO). We would like to thank Anthony Olivieri for his help with fabrication.